Biomedicine & Pharmacotherapy 204 (2026) 119961

Contents lists available at ScienceDirect

Biomedicine & Pharmacotherapy

journal homepage: www.elsevier.com/locate/biopha

Transient ultrastructural remodeling of the open canalicular system and α-granules is associated with endothelial responses after BNT162b2 vaccination in healthy volunteers

Valentina Carlini [a], Emilio Trabucchi [b], Nadia Santo [c], Norma Lattuada [c], Stefania Saccucci [c], Raffaele Allevi [d], Francesca Rispoli [a], Barbara Bianchi [a], Ermanno Longhi [a], Maria Belen Macas Granizo [e], Marco D'Anzeo [f], Cesare Berra [a], Angelo Naselli [a], Alberto Settembrini [a], Elena Tagliabue [a], Elena Vianello [e,g], Elena Dozio [e,g], Massimiliano Corsi Romanelli [e,h], Antonio E. Pontiroli [i], Martino Bolognesi [c,1], Lucia La Sala [a,e,*,1,2]

[a] IRCCS MultiMedica, Via Fantoli 16/15, Milan 20138, Italy
[b] Fondazione MultiMedica ETS, Via Fantoli 16/15, Milan 20138, Italy
[c] UNITECH NOLIMITS – University Technological Platform, University of Milan, Via Golgi 19, Milan 20133, Italy
[d] University of Milan, Dept of Biomedical Sciences and Clinic, Milan 20157, Italy
[e] University of Milan, Dept of Biomedical Sciences for Health, Milan 20133, Italy
[f] AUO delle Marche, SOD Medicina di Laboratorio, Ancona 60100, Italy
[g] Experimental Laboratory for Research on Organ Damage Biomarkers, IRCCS Istituto Auxologico Italiano, Milan Italy
[h] Department of clinical and experimental pathology, IRCCS Istituto Auxologico Italiano, Milan Italy
[i] University of Milan, Dept of Health Science, Milan 20146, Italy

ARTICLE INFO

Keywords:
Platelet priming
MRNA vaccination
Transmission electron microscopy
Open canalicular system
α-granules
Endothelial activation

ABSTRACT

Platelets are key coordinators of hemostatic and immune functions, rapidly responding to vascular perturbations. However, the ultrastructural signatures of platelet priming, including open canalicular system (OCS) remodeling and α-granule (αG) changes, remain poorly characterized. BNT162b2 vaccination induces a well-defined, self-limiting immune activation in healthy individuals, providing a controlled human model to investigate platelets and vascular responses. Using this model, we longitudinally investigated platelet ultrastructure, assessing alterations in OCS architecture and αG content and their association with circulating inflammatory and endothelial activation biomarkers. Healthy adults were evaluated at six time points across two BNT162b2 vaccine doses. Platelets were analyzed by TEM to quantify αG number and OCS area in a participant subcohort. Circulating levels of IL-6, CD40L, P-selectin and plasminogen activator inhibitor-1 (PAI-1) were measured by ELISA in the full cohort. Human umbilical vein endothelial cells (HUVECs) were stimulated with post-vaccination plasma to assess endothelial responses. Vaccination induced transient OCS expansion and αG depletion, accompanied by transient systemic immune activation, as reflected by changes in circulating IL-6, CD40L, and PAI-1, whereas P-selectin showed no sustained increase, consistent with a primed/intermediate activation state. Post-vaccination plasma induced dynamic changes in HUVECs IL-1Rs, MIP-3α, and IL-22 secretion, adhesion molecules and chemokine transcription, and 14–3–3γ, P2Y12, PAI-1, and ADAMTS13 signaling, consistent with transient endothelial activation. BNT162b2 vaccination thus elicits coordinated, non-pathological platelet remodeling alongside transient systemic and endothelial responses. OCS and αG may represent sensitive ultrastructural indicators of transient platelet activation, defining a novel morpho-functional signature of vaccine-induced immune activation at the vascular interface.

* Correspondence to: Dept of Biomedical Sciences for Health, Via Mangiagalli 31, Milan 20133, Italy.
E-mail address: lucia.lasala@unimi.it (L. La Sala).
[1] The authors contributed equally
[2] IRCCS MultiMedica, PST Via Fantoli 20138, Milan (Italy).

https://doi.org/10.1016/j.biopha.2026.119961
Received 2 May 2026; Received in revised form 18 August 2026; Accepted 27 September 2026
Available online 29 September 2026
0753-3322/© 2026 The Authors. Published by Elsevier Masson SAS. This is an open access article under the CC BY-NC license (http://creativecommons.org/licenses/by-nc/4.0/).

1. Introduction

Platelets (PLT) are increasingly recognized as active sentinels of immune surveillance and vascular homeostasis, acting at the intersection of coagulation, inflammation, and endothelial integrity. However, the precise mechanisms distinguishing transient, protective platelet remodeling during physiological immune response from pathological platelet activation in thrombo-inflammation remain incompletely defined.

PLT are anucleate cytoplasmic fragments released from megakaryocytes (MK), specialized myeloid-lineage cells whose maturation and proplatelet formation are primarily regulated by thrombopoietin (TPO) [1]. Classically, PLT are involved in primary hemostasis through adhesion to exposed sub-endothelial matrix, cytoskeletal remodeling, aggregation and regulated granule secretion at the site of vascular injury. Beyond their canonical role in thrombosis, they contribute to vascular homeostasis by releasing a multitude of bioactive mediators such as cytokines and chemokines, growth factors, and immunomodulatory molecules from their α-granules (αG) that drive inflammatory and immune responses [2]. Notably, despite lacking a nucleus, platelets preserve a rich signaling apparatus and highly organized organelle architecture that allow rapid structural and functional adaptation in response to inflammatory perturbations.

The capacity of platelets to bridge hemostasis and immunity is grounded in both molecular and cellular features. Through the expression and release of immunomodulatory mediators and adhesion molecules, such as CD40 ligand (CD40L) and P-selectin, platelets engage endothelial and leukocyte partners, contributing to both immune surveillance and vascular repair [1,3–6]. This hemostatic-immune crosstalk defines the emerging paradigm of immune-thrombosis, in which platelets act as dynamic transducers and coordinators of inflammatory signals within the circulation [7–9]. A central unresolved question is how to capture the "physiological" end of this spectrum and identify a potentially reversible intermediate state in which platelets undergo transient adaptive remodeling without progressing to full activation or sustained secretion, thereby distinguishing it from maladaptive thrombo-inflammation. In the present study, we refer to this putative intermediate condition as "platelet priming" and we aimed to determine whether specific ultrastructural changes are consistent with such an adaptive phenotype.

In this scenario, the widespread administration of BNT162b2 mRNA-based immunization against SARS-CoV-2 provided a controlled human model to investigate how physiological immune activation transiently modulates platelet biology. While large clinical trials support overall safety of BNT162b2 vaccine [10–13], several studies report short-lived fluctuations in platelet count, inflammatory cytokines, and pro-thrombotic mediators, all of which remain within physiological ranges [14]. Longitudinal single-cell and immunological profiling after BNT162b2 vaccination has shown that anti-Spike antibody responses peak after the second vaccine dose, decline over time, and are restored by booster administration, along with persistent Spike-specific memory B-cell and effector/effector-memory T-cell responses, supporting a time-resolved and self-limited pattern of immune activation [15].

These observations raise the possibility that platelets and vascular endothelium may temporarily undergo a reversible remodeling process during vaccination-induced immune activation, a physiological phenomenon fundamentally distinct from pathological thrombosis. The biological mechanisms underlying this transient adaptation remain, however, largely unexplored.

Traditional markers of platelet activation, including soluble mediators (e.g., P-selectin and CD40L), as well as platelet count variations, capture only part of the response and may fail to detect subcellular remodelling events that accompany the transient priming state. Two platelet compartments are particularly informative for investigating this process: the open canalicular system (OCS), a network of membrane invaginations supporting secretion and membrane surface expansion, and α-granules (αG), which store a repertoire of pro- and anti-thrombotic proteins crucial for hemostasis and immune modulation [16–19]. Monitoring structural remodeling of platelet membrane and secretory compartments, including changes in the OCS architecture and αG content, may provide a more sensitive window into this intermediate state and help define the time-resolved signature of platelet-vascular immune adaptation. Importantly, transmission electron microscopy (TEM) remains the reference technique to quantify distinct platelet ultrastructural abnormalities [20], including alterations in size, shape, αG, OCS and Golgi complex and presence of aberrant inclusions. Accordingly, it is routinely used to differentially diagnose many inherited platelet disorders such as Gray platelets syndrome, Hermansky–Pudlak syndrome, Wiskott–Aldrich syndrome, and Chediak–Higashi syndrome, among others [21–24].

Based on these observations, we performed a longitudinal analysis of platelet-endothelial remodeling during BNT162b2 immunization of healthy subjects, integrating platelet ultrastructural metrics with circulating thrombo-inflammatory mediators and in vitro endothelial cell responses to post-vaccination plasma. By defining the temporal coordination of these ultrastructural and molecular readouts, we aim to delineate a morphofunctional signature of transient, vaccine-induced, self-limited vascular immune activation.

2. Material and methods

2.1. Study design and procedures

An age- and gender- mixed group of individuals, not previously affected by SARS-CoV-2 infection (Supplementary Table S1 and S2), were enrolled as volunteer donors in the CORE study, after providing written informed consent. The CORE study has been approved by the Board of Independent Ethics Committee of the IRCCS MultiMedica, Milan, Italy (application number 470.2021, CE-40.2021). During the study, whole blood samples were repeatedly collected from each participant by venipuncture at six different time points from February 2021 through May 2021: the first immediately before the administration of BNT162b2 mRNA-based vaccine (baseline, T0), then the day after the first dose of BNT162b2 vaccine (T1), 1 week (T2) and 2 weeks (T3) later, the day after the second dose of BNT162b2 vaccine (also called booster, T4), and 1 week (T5) after the administration of vaccination booster (Supplementary Fig. S1).

2.2. Human samples preparation for ELISA assays and TEM procedures

Samples were obtained from blood of vaccinated healthy subjects as follows: a) Serum samples were collected from whole blood samples in anticoagulant-free tubes and left to clot at room temperature for 15–30 min. The clot was removed by centrifuging at 1000–2000 x g for 10 min and the resulting supernatant (serum) was transferred into new tubes and stored at –80°C; b) Plasma samples were collected from whole blood samples in EDTA-treated tubes and centrifuged at 1000–2000 x g for 10 min for successful separation of blood cells. The resulting supernatant (plasma) was transferred into clean tubes and stored at −80 °C, or further centrifuged at 2500 x g for 15 min, to obtain platelet-depleted plasma and platelet pellets (PLT), which were both stored at −80°C.

Among the forty-six participants, a subset of thirteen subjects (n = 13 per time point, Table 1) were used for platelet ultrastructural analyses by TEM.

2.3. Transmission Electron Microscopy (TEM)

Fresh human platelets were obtained by differential centrifugation of whole blood (collected in vacutainer containing 1 mM EDTA) at 2500 rpm for 15 min. Platelets were washed with cold PBS 1:5 to discard any contamination, followed by a second centrifugation at 2500 rpm for

Table 1
Anthropometric characteristics of the study cohort at baseline (T0), after the first (T1) and second (T4) dose.

Time-points	T0	T1	T4
Parameters	**mean (±SD)**	**mean (±SD)**	**mean (±SD)**
Age, y	36.05 ± 2.2	-	-
Sex			
woman (N, %)	32 (69.6%)	-	-
man (N, %)	14 (30.4%)	-	-
WBC (10^3/uL)	7.3 ± 1.7	7.4 ± 1.6	6.9 ± 2.0
RBC (10^6/uL)	4.8 ± 0.4	4.7 ± 0.4	4.6 ± 0.4
Hgb (g/dL)	14.1 ± 1.3	13.9 ± 1.3	13.6 ± 1.4
HCT (%)	42.8 ± 3.4	42.4 ± 3.5	41.9 ± 3.4
MCV (fL)	90.3 ± 4.3	90.4 ± 4.4	91.2 ± 4.8
MCHC (g/dL)	32.8 ± 0.9	32.7 ± 0.9	32.5 ± 0.9
MCH (pg)	29.6 ± 1.5	29.6 ± 1.6	29.6 ± 1,6
PLT (10^3/uL)	250.1 ± 51.7	240.7 ± 54.7	241.3 ± 47.3
P-LCR (%)	31.8 ± 7.7	31.9 ± 7.0	29.2 ± 6.0
MPV (fL)	10.9 ± 1.0	10.8 ± 0.8	10.5 ± 0.7
PDW (fL)	13.2 ± 2.4	13.1 ± 1.8	12.2 ± 1.6
PCT (%)	0.3 ± 0.0	0.3 ± 0.1	0.3 ± 0.0
Neutrophils (10^3/uL)	4.3 ± 1.5	4.8 ± 1.3	4.7 ± 1.8
Basophils (10^3/uL)	0.04 ± 0.02	0.04 ± 0.02	0.04 ± 0.02
Eosinophils (10^3/uL)	0.14 ± 0.11	0.12 ± 0.11	0.14 ± 0.12
Lymphocytes (10^3/uL)	2.3 ± 0.6	1.9 ± 0.6	1.5 ± 0.5
Monocytes (10^3/uL)	0.5 ± 0.1	0.6 ± 0.1	0.6 ± 0.2

WBC: whole blood cell; RBC: red blood cell; Hgb: haemoglobin; HCT: haematocrit; MCV: mean corpuscular value; MCHC: mean corpuscular haemoglobin concentration; MHC: mean corpuscular haemoglobin; PLT: platelets; P-LCR: platelet-larger cell ratio; MPV: mean platelet volume; PDW: platelet distribution widht; PCT: plateletcrit.

5 min. The platelet pellets were immediately fixed in 2.5% glutaraldehyde in 0.12 M sodium cacodylate buffer to preserve platelet ultrastructure and stored at 4°C. After centrifuging at 3000 rpm for 3 min and discarding the supernatant, the pellets were resuspended with 8% bovine serum albumin (BSA) in 0.12 M sodium cacodylate buffer and centrifuged at 5000 rpm for 5 min. A second fixation step by adding 2.5% glutaraldehyde in 0.12 M sodium cacodylate buffer was performed to stabilize the platelet pellet, which were then gently resuspended and centrifuged at 5000 rpm for 10 min. Following washing, they were further fixed in 1.5% osmium tetroxide, rinsed, dehydrated, and embedded in an Epon-Araldite resin.

Ultrathin sections (70–80 nm) of Epon-embedded platelets were cut with a PowerTome XL RMC ultramicrotome and stained with uranyl acetate and lead citrate, then imaged under a Talos L120C transmission electron microscope (Thermo Fisher Scientific) at 120 kV. Images were acquired at a final magnification of 13,500x using a Ceta CMOS Camera (Thermo Fisher Scientific) and analyzed with ImageJ software (NIH Image). Given the resource-intensive nature of TEM, ultrastructural analyses were performed in a pre-specified subcohort (n = 13), selected from the overall cohort (n = 46). TEM micrographs were used to measure the total platelet area (μm^2) and the main internal compartments (number of αGs and area of OCS (μm^2)). For each of the thirteen (n = 13) participants, eighteen (n = 18) platelets were analyzed at each of the six time points, corresponding to an overall dataset of 1404 platelets (13 participants × 18 platelets × 6 time points) across the entire longitudinal study.

Platelets were selected using a fully random sampling approach, without selection based on image quality or morphological features and both image acquisition and morphometric analyses were performed blinded to the experimental time points.

2.4. Enzyme-linked immunosorbent assay

Forty-six serum samples, obtained as previously described, were analyzed by solid-phase sandwich enzyme-linked immunosorbent assay (ELISA), according to the manufacturer's protocol, to determine the circulating levels of human interleukin 6 (IL-6), soluble P-selectin (sP-selectin), soluble CD40 ligand (sCD40L). For IL-6 (Human IL-6 ELISA Kit, catalog n. BMS213–2, Invitrogen, Thermo Fisher Scientific, USA) and soluble P-selectin (Human sP-selectin ELISA kit, catalog n. BMS219–4, Invitrogen, Thermo Fisher Scientific, USA) samples were diluted 1:2 and 1:10, respectively, and analyzed by DSX Automated ELISA Processing System (Dynex Technologies, USA) measuring absorbance at 450 nm.

For both CD40L (Human CD40 Ligand/TNFSF5 Quantikine ELISA Kit, catalog n. DCDL40, R&D Systems, USA) and PAI-1 (Human PAI-1 ELISA Kit, catalog n. BMS2033, Invitrogen, Thermo Fisher Scientific, USA) samples were diluted 1:5 and analyzed in duplicate by a microplate spectrophotometer (SPECTROstar Nano, BMG LABTECH, Germany) reading the absorbance at 450 nm as primary wavelength, and at 540 nm and 620 nm, respectively, as reference wavelength. Protein concentration for each sample was determined by interpolation with a standard curve using a 4-paramenter logistic (4PL) curve-fitting statistical software.

2.5. HUVECs maintenance and stimulation

Primary pooled human umbilical vein endothelial cells (HUVECs, CC-2519) and growth factors were purchased from Lonza (Lonza Bioresearch LBS, Basel, Switzerland). Cells were cultured in endothelial basal medium (EBM-2), supplemented with low foetal bovine serum (2%), hydrocortisone (1 μg/mL), human basic fibroblastic growth factor (bFGF, 5 ng/mL), recombinant human epidermal growth factor (rhEGF, 5 ng/mL), heparin (0.75 units/mL) and gentamicin/amphotericin-B (GA-1000, 0.1%) in a humidified incubator at 37°C with 5% CO_2.

Cells were used at passage 4 (p4) and seeded in 6-well plates at a density of 2×10^5 cells/well. Once 80–90% confluence was reached, cells were stimulated with 10% (v/v) pooled plasma collected at time points T0-T5 from vaccinated subjects, in complete EBM-2 medium for 6 h at 37°C. For each time point, two independent plasma pools were constituted, each consisting of plasma samples from three different donors (n = 3); the same donor combinations were maintained across all time points. Each plasma pool was independently tested in duplicate wells, and the entire experiment was repeated two times.

2.6. HUVEC cytokine secretome profiling

The cell culture supernatant from unstimulated (NT) or stimulated HUVEC (T0-T5) was collected, pooled for each time point, and analyzed using a RayBio® Human Cytokine Antibody Array (AAH-TH17–1, RayBiotech, Inc, Norcross, GA, USA) for the semi-quantitative detection of 34 human cytokines, including Th1-, Th2-, and Th17-related cytokines, following the manufacturer's protocol. Briefly, array membranes were incubated with samples overnight at 4°C, washed, and incubated with biotin-conjugated detection antibodies. After incubation with HRP-conjugated streptavidin and chemiluminescent detection, images were acquired by Alliance Q9 ATOM (Uvitec, Cambridge, UK) and signal density was analyzed by ImageJ software (NIH, Bethesda, MD, USA) using Gilles Carpentier's Protein Array Analyzer tool for ImageJ (http://image.bio.methods.free.fr/dotblot.html). The relative concentration of each cytokine in the samples was calculated by normalizing the signal density of each cytokine spot to internal positive control spots using RayBio® Analysis Tool software.

2.7. Western blot analysis

For western blot analysis, HUVECs were lysed in RIPA buffer (Sigma-Aldrich) supplemented with 1% protease and 1% phosphatase inhibitor cocktails (Sigma-Aldrich). Total protein content was determined using Bradford assay (Sigma-Aldrich), and 30 μg of protein was separated by electrophoresis using 4–12% NuPAGE Bis-Tris protein gels (Invitrogen) and transferred onto a PVDF membrane (GE Healthcare,

Buckinghamshire, UK). Membranes were blocked with 5% bovine serum albumin and incubated overnight at 4°C with the following primary antibodies: PAI-1 (11907) (1:1000; Cell Signaling Technology), 14–3–3γ (ab137048), P2Y12 (ab233760) and ADAMTS13 (ab177940) (all 1:1000; Abcam). Specific primary antibodies are listed in Table 5. Following incubation with appropriate secondary horseradish peroxidase-conjugated IgG antibodies (1:3000, GE Healthcare Europe GmbH, Milan, Italy) for 1 h at room temperature, blots were revealed by enhanced chemiluminescence (ECL) system (Thermo Scientific, Rockford, IL, USA), with Alliance Q9 Atom System (Uvitec, Cambridge, UK). Proteins were quantified by ImageJ software (NIH, Bethesda, MD, USA). Human β-actin (1:2000, Cell Signaling Technology) was used as a loading control.

2.8. RNA extraction and real-time PCR analysis

Total RNA was extracted from HUVECs using a commercial RNA purification kit (Norgen Biotek, Thorold, ON, Canada) following the manufacturer's protocol. 1 microgram of total RNA was reverse transcribed using SuperScript VILO cDNA synthesis kit (Invitrogen, Thermo Fisher Scientific, NY, USA) according to the manufacturer's instructions. Real-time qPCR (RT-qPCR) was performed using SYBR Green reagent (TaKaRa Bio Company, Clontech, Mountain View, CA, USA) on QuantStudio 6 Flex (Applied Biosystems, Foster City, CA, USA) detection system. Specific primers are listed in Table 6. For all RT-qPCR results, the relative gene expression was normalized to β-actin. Data were obtained as Ct values, and the $2^{-\Delta Ct}$ method was used in the analysis.

2.9. Statistical analysis

Data were reported as mean (standard error) or median and interquartile range (IQR) for continuous variables and as absolute or relative frequencies for categorical variables. Chi-squared or Fisher exact test, Wilcoxon rank test or Kruskal-Wallis rank sum test were used to investigate the association between vaccination responses and haematological parameters.

Differences in continuous variables between time points were evaluated by mixed models for repeated measures. Association between variables at specific time points was evaluated by linear regression model. Analyses were performed using SAS software (Version 9.4; SAS Institute Inc., Cary, NC, USA). For in-vitro analysis we used GraphPad Prism (version 11.0.1 for Windows, GraphPad Software, Boston, MA, USA), with multiple correction post-hoc analysis. Data were considered statistically significant for p-values < 0.05.

3. Results

3.1. Platelet ultrastructural changes during vaccination time course

3.1.1. Absence of viral particles in platelets

mRNA-based vaccination has the advantage of being virus-free. Since platelets can be infected by SARS-CoV-2 variants [25], we first investigated the presence of viral particles in platelets. By TEM, we morphologically examined the content of eighteen platelets at each study time point from each of the thirteen participants selected for ultrastructural analyses. We could not observe any viral particles in the analyzed samples, as indicated by the absence of their characteristic crown-like structure.

3.1.2. Platelet-Ultrastructural changes are indicative of platelet activation during the immunization process against SARS-CoV-2

Ultrastructural analysis conducted on platelets from participants who received the Pfizer BNT162b2 mRNA vaccine revealed changes in the expansion of the OCS and in the number of αGs (Fig. 1, Fig. 2 A-B). TEM analysis showed distinct platelet features in the analyzed subcohort of selected healthy donors who participated in the immunization campaign. In particular, the OCS area appeared progressively expanded, reaching a peak at T3 (T3, $p < 0.05$ vs T0, $p < 0.0001$ vs T1 and T2) and then declined, returning to baseline levels (Fig. 2 A). The temporary presence of enlarged OCS during the immunization period (first and second doses) may be related to a transient platelet activation. Moreover, the αG number decreased during the study period with respect to T0 and significantly increased at T5 (Fig. 2 B). In addition, when comparing the effect of vaccination at the time points associated with

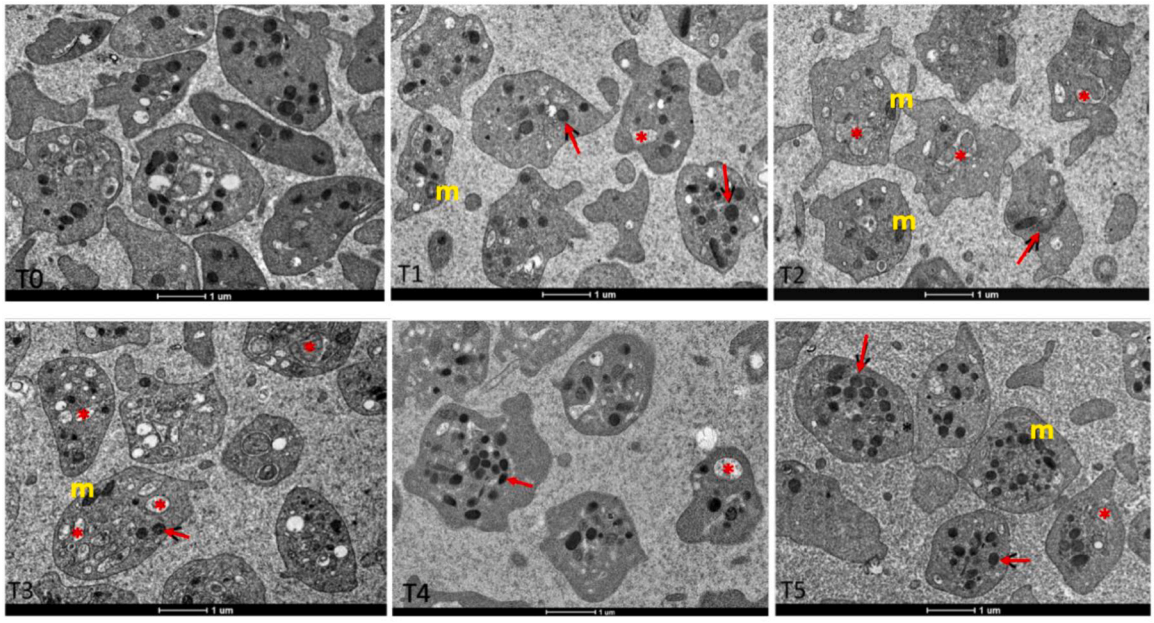

Fig. 1. Ultrastructural remodeling of the open canalicular system (OCS) and α-granules (αG) in circulating platelets following BNT162b2 vaccination. Representative transmission electron microscopy (TEM) images of circulating platelets collected at baseline (T0), after the first vaccine dose (T1–T3), and following the second dose (T4–T5). Platelets show a transient OCS expansion (**red asterisks**) and a concomitant reduction in αG number (**red arrows**) at early time points (T1–T3), returning to baseline morphology by T5. Legend: Arrows, alpha-granules; *, open canalicular system (OCS); m, mitochondria; scale bar = 1 μm.

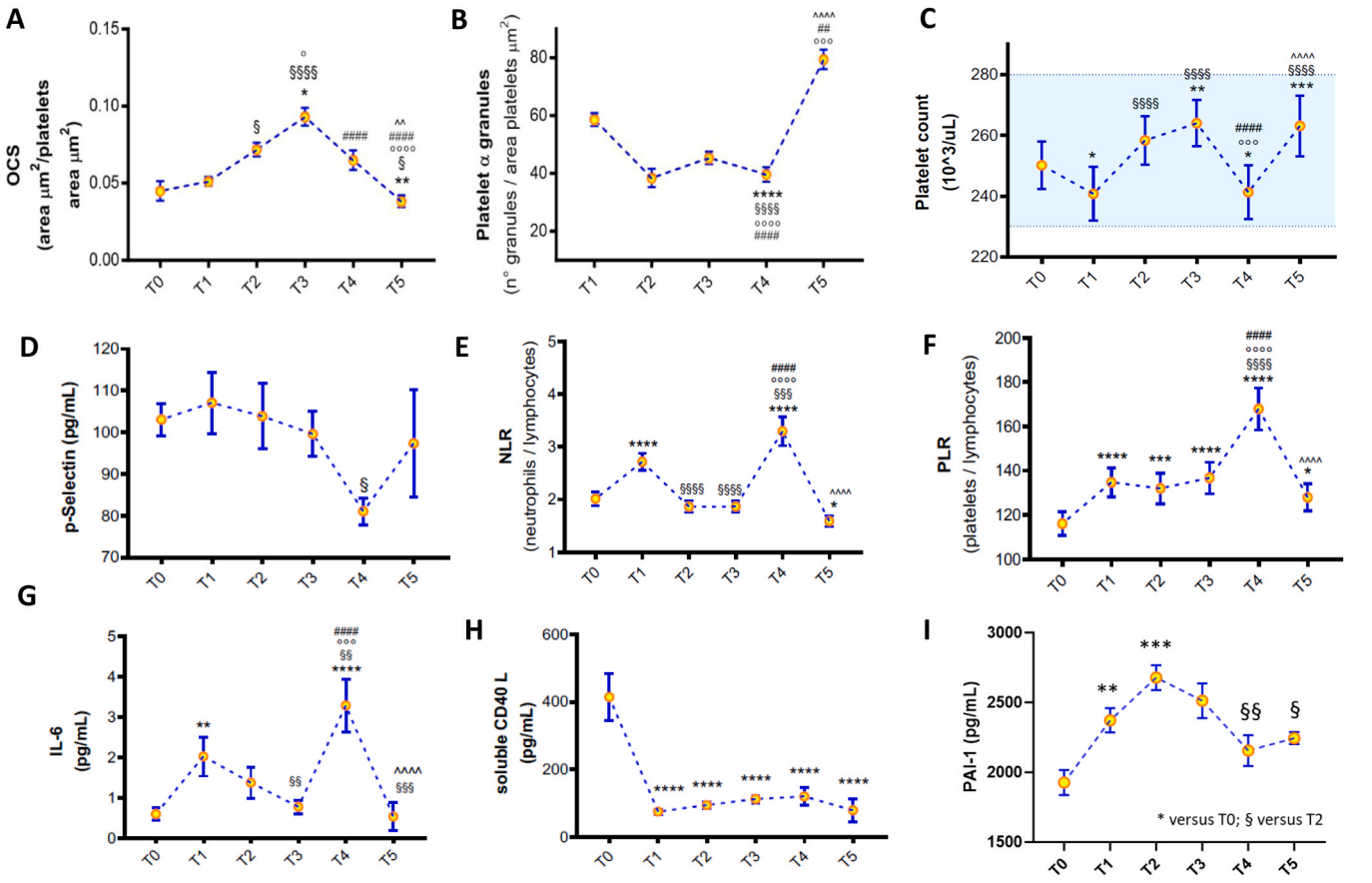

Fig. 2. Longitudinal analysis of platelet during BNT162b2 mRNA vaccination. A-B. Quantitative analysis of OCS area (left) and αG count per platelet (right) at each time point (T0–T5). Data represent mean ± SEM; 18 platelets/donors/time point were analyzed (n = 13 donors). A transient increase in OCS area and a parallel decrease in αG number were observed after the first dose, consistent with a non-degranulating primed platelet phenotype. Differences in continuous variables between time points were evaluated by mixed models for repeated-measures, using SAS software (Version 9.4; SAS Institute Inc., Cary, NC, USA) procedures PROC MIXED. Legend: * vs T0, § vs T1, ° vs T2, # vs T3, ^ vs T4; $p < 0.05$, $p < 0.01$, $p < 0.001$, $p < 0.0001$. **C.** Platelet count (10^3/µL) was measured in 46 healthy, SARS-CoV-2–naïve individuals at six time points spanning the two-dose BNT162b2 vaccination schedule (T0–T5). Platelet count was within the range of normality (blue light area) defined by range 150–400 × 10^9/L. In T1 and T4, corresponding at the first and second doses of vaccine, count is significantly reduced compared to pre-vaccination baseline (T0 = no vaccination). A transient decrease in platelet number was observed after the first dose (T1–T2), followed by recovery and stabilization post-second dose (T4–T5). Data were expressed as mean ± SEM. Statistical comparisons were performed using repeated-measures ANOVA with post hoc correction; symbols indicate significance between time points as specified in the figure. Differences between time points were evaluated by mixed models for repeated-measures, using SAS software (Version 9.4; SAS Institute Inc., Cary, NC, USA) procedures PROC MIXED. Sample size: n = 44 T0; n = 39 T1; n = 37 T2; n = 38 T3; n = 29 T4; n = 31 T5. Legend: * vs T0, § vs T1, ° vs T2, # vs T3, ^ vs T4. $p < 0.05$, $p < 0.01$, $p < 0.001$, $p < 0.0001$. **D-I. Systemic markers of inflammation and platelet activation following BNT162b2 vaccination.** Circulating levels of P-selectin (D), IL-6 (G), soluble CD40L (H) and PAI-1(I) were measured by ELISA at six time points during the two-dose BNT162b2 mRNA vaccination schedule (T0–T5). Data are presented as mean ± SEM. Statistical comparisons among time points were performed using repeated-measures ANOVA with post hoc testing; significance is indicated in the figure. **D.** Serum concentration of soluble P-selectin (pg/mL), a marker of platelet activation and aggregation, was evaluated during immunization time points (n = 18 T0; n = 12 T1; n = 11 T2; n = 16 T3; n = 11 T4; n = 18 T5). P-selectin levels were strongly reduced following booster administration ($p < 0.05$ vs T1). **E.** Neutrophil to lymphocyte ratio (NRL) significantly increased at the first ($p < 0.0001$) and second dose ($p < 0.0001$) compared with baseline. **F.** Platelet to lymphocyte ratio (PLR) showed a tendency to progressively increase over time, reaching a peak concomitant with the second vaccine dose ($p < 0.0001$ vs all other time points). The ratio significantly decreased 1 week after booster administration ($p < 0.0001$ vs T4). Differences among time points were evaluated by mixed-effects models for repeated-measures, using SAS software (Version 9.4; SAS Institute Inc., Cary, NC, USA) procedures PROC MIXED. Sample size: n = 44 T0; n = 39 T1; n = 37 T2; n = 38 T3; n = 29 T4; n = 31 T5. **G.** Serum concentration of the inflammatory marker interleukin-6 (IL-6, pg/dL; n = 18 T0; n = 12 T1; n = 11 T2; n = 16 T3; n = 11 T4; n = 18 T5) significantly increased after the first ($p < 0.01$) and second vaccine doses ($p < 0.0001$). After the booster, IL-6 amounts decreased significantly ($p < 0.0001$ vs T4). **H.** Serum concentration of soluble CD40 ligand (sCD40L, pg/mL), a marker of platelet activation, was evaluated during the immunization time points (n = 8 T0; n = 7 T1; n = 6 T2; n = 6 T3; n = 6 T4; n = 6 T5). **I.** Serum concentration of plasminogen-activator inhibitor-1 (PAI-1, pg/mL), a platelet-associated pro-thrombotic mediator acting as a fibrinolysis inhibitor, was measured during immunization schedule (n = 18 T0; n = 12 T1; n = 11 T2; n = 16 T3; n = 11 T4; n = 18 T5). Differences between time points were evaluated by mixed-effects models for repeated-measures, using SAS software (Version 9.4; SAS Institute Inc., Cary, NC, USA) procedures PROC MIXED. Legend: * vs T0, § vs T1, ° vs T2, # vs T3, ^ vs T4; $p < 0.05$, $p < 0.01$, $p < 0.001$, $p < 0.0001$ respectively.

vaccine administration (T1 and T4), we observed a significant positive association between the increase of αG number and platelet count at T1 ($p < 0.01$; Table 2). In particular, after the first dose (T1), for every 10-unit increase in platelet count, the number of granules significantly increased by 0.084 units ($p = 0.0012$). Conversely, after the booster dose (T4), we observed an apparent decrease in αG number for every 10-unit increase of platelet count, although this association did not reach statistical significance ($p = 0.9$).

Mean platelet count was significantly lower after vaccine administration (T1 and T4, $p < 0.05$ vs baseline T0; Table 1, Fig. 2 C) and progressively increased during the immunization process, reaching higher values at T3 ($p < 0.01$ and $p < 0.0001$ vs T0 and T1, respectively). Although the platelet count underwent these variations across the different time points, it remained within the normal range

Table 2
Multivariable mixed-effects models evaluating platelet and inflammatory parameters across time points.

Outcome	Independent variable	T1		T4	
		Estimate	p-value	Estimate	p-value
αG number	OCS	-1.393	0.9229	-15.801	0.5583
αG number	P-selectin*	0.002	0.9795	-0.519	0.072
αG number	CD40*	-0.121	0.3104	-0.018	0.8787
αG number	Platelet count *	0.084	**0.0012**	-0.008	0.9371
Platelet count	IL-6	1.958	0.8533	-3.538	0.676
Platelet count	OCSˆ	15.992	0.3187	11.666	0.2248
Platelet count	RBC°	-1.762	0.389	-2.52	0.236
*10-unit increase					
ˆ0.01-unit increase					
°0.1-unit increase					

For each unit increase in the independent variable, the outcome increases/decreases by a value equal to the estimate at the time indicated in the column.
OCS: open canalicular system; CD40: cluster domain 40; IL-6: interleukine-6; RBC: red blood cells.

(150–400 $\times 10^9$/L, Fig. 2 C) throughout the study period.

3.1.3. Absence of significant changes in α-granule secretion

Soluble P-selectin, a thrombo-inflammatory protein involved in platelet activation, aggregation and thrombus formation [26], is released into the circulation upon platelet activation and is widely considered as a first-choice marker of αG secretion [27]. To quantify α-granule protein release, the levels of soluble P-selectin were analyzed by ELISA in serum samples from vaccinated subjects. P-selectin levels (Fig. 2 D) remained largely stable during the experimental period, but significantly decreased in response to the booster vaccination (T4, $p < 0.05$), followed by a gradual return toward baseline levels in the subsequent days (T5) (Fig. 2D).

Regression models for individual time points (T1 and T4, corresponding to first and second vaccine doses) showed a tendency toward an inverse association between αG number and P-selectin levels, although this did not reach statistical significance ($p = 0.07$; Table 2).

The marker of systemic inflammation Neutrophil to lymphocyte ratio (NLR) significantly increased after the first ($p < 0.0001$) and second doses ($p < 0.0001$), compared to T0 (Fig. 2 E). Similarly, another marker of inflammation, the Platelet to lymphocyte ratio (PLR), showed a significant increase over time (T1 vs T0, $p < 0.0001$; T2 vs T0, $p < 0.001$; T3 vs T0, $p < 0.0001$), reaching a significant peak concomitant with the second dose ($p < 0.0001$, Fig. 2 F).

3.1.4. Platelet parameters linked to the expansion of OCS

In Table 3, mixed effect models found significant associations between OCS area and mean platelet volume (MPV; $p = 0.014$), platelet-larger cell ratio (P-LCR; $p = 0.011$), and platelet distribution width (PDW; $p = 0.016$). These results suggest that size-based platelet parameters are more susceptible to OCS remodeling in comparison with platelet count, consistent with their higher sensitivity to alterations in platelet morphology and activation state [28].

3.2. Dynamic changes in circulating levels of pro-inflammatory IL-6, CD40L, and pro-thrombotic PAI-1 during vaccination time course

To evaluate whether the administration of BNT162b2 vaccine could induce pro-inflammatory and pro-thrombotic responses, serum levels of IL-6, CD40L and plasminogen activator inhibitor-1 (PAI-1), three proteins playing a key role in inflammation, platelet activation and thrombosis, were quantified by ELISA at baseline and subsequent time points. Notably, the pro-inflammatory cytokine IL-6 may trigger platelet activation and coagulation [29,30].

Table 3
Mixed-effect models on blood-based platelet parameters.

OCS outcome					
Effect	**SE**	**P-value**	**Effect**	**SE**	**P-value**
Intercept	0.05	0.0003	**Intercept**	0.11	< .0001
PCT	0.06	0.1210	**PDW**	-0.003	0.0168
T0	Ref	-	**T0**	Ref	-
T1	-0.11	0.09	**T1**	-0.01	0.10
T2	-0.002	0.81	**T2**	0.004	0.64
T3	0.02	0.03	**T3**	0.02	0.01
T4	-0.008	0.37	**T4**	-0.003	0.71
T5	-0.03	0.003	**T5**	-0.03	0.002
Effect	**SE**	**P-value**	**Effect**	**SE**	**P-value**
Intercept	0.10	< .0001	**Intercept**	0.15	< .0001
P-LCR	-0.0009	0.0112	**MPV**	-0.007	0.0145
T0	Ref	-	**T0**	Ref	-
T1	-0.17	0.097	**T1**	-0.018	0.080
T2	0.0038	0.71	**T2**	0.002	0.822
T3	0.022	0.024	**T3**	0.0224	0.029
T4	-0.0046	0.65	**T4**	-0.005	0.61
T5	-0.033	0.0014	**T5**	-0.034	0.0014

OCS: open canalicular system; PCT: plateletcrit %; PDW: platelet distribution widht fL;
MPV: mean platelet volume fL; P-LCR: platelet-larger cell ratio (%).

In Fig. 2 G, compared to baseline (T0), IL-6 levels were significantly increased following the administration of the first dose of anti-SARS-CoV-2 vaccination (T1, $p < 0.01$), and gradually returned to baseline values during the subsequent weeks (T2, T3 $p < 0.01$). IL-6 levels underwent a further significant increase concomitant with the administration of the vaccine booster (T4, $p < 0.0001$), returning then to baseline levels (T5) within one week (Fig. 2G). These data are consistent with a transient, self-resolving immune response associated with vaccination.

CD40L is stored in αG and primarily released upon platelet activation, acting as a key inducer of immune reactivity and inflammation [31,32]. Soluble CD40L concentration was higher at baseline (T0) and significantly decreased after the first vaccination dose (T1, $p < 0.0001$), remaining low throughout the subsequent time points (T2-T5, $p < 0.0001$) (Fig. 2 H). These data suggest that circulating platelets exhibited a physiological state of immune reactivity and that BNT162b2 administration did not induce a sustained CD40L-mediated platelet activation, but rather a transient and tightly regulated platelet immune response.

In Fig. 2 I, circulating PAI-1 levels showed dynamic changes during the vaccination time course. Relative to baseline (T0), PAI-1 concentrations significantly increased at T1 ($p < 0.01$ vs T0) and reached a peak at T2 ($p < 0.001$ vs T0), remaining elevated at T3. Thereafter, PAI-1 levels declined during the later phases of the immunization time course, with the values at T4 and T5 significantly lower than those at T2 ($p < 0.01$ and $p < 0.05$ vs T2, respectively). Overall, these data indicate a time-resolved, self-limiting modulation of circulating PAI-1 during BNT162b2 immunization.

3.3. Transient activation of the IL-1/IL-6 signaling axis in endothelial cell secretome

To investigate whether plasma from vaccinated individuals harbors soluble mediators capable of activating endothelial cells, we exposed primary human umbilical vein endothelial cells (HUVECs) for 6 h to normal medium (not treated, NT) or to medium supplemented with 10% plasma collected longitudinally from healthy donors at six defined time points (T0- T5) following BNT162b2 administration. Endothelial secretome responses were assessed using a semi-quantitative multiplex cytokine antibody array performed on pooled supernatants for each group.

Visual quantification of array spot intensities (Fig. 3 A-B, Table 4) revealed a coordinated and temporally regulated cytokine and soluble receptor secretion profile.

Notably, as reported in Fig. 3 B, HUVECs stimulated with plasma collected at early post-vaccination time points (acute phase, T1–T3) showed elevated release of IL-6 ($p < 0.01$ vs T0), soluble IL-6 receptor (sIL-6R, $p < 0.01$), and soluble gp130 (sgp130, $p < 0.01$) - suggestive of engagement and early transient activation of both canonical IL-6 signaling and IL-6 trans-signaling pathways. The signal for sgp130 decreased at T3 ($p < 0.01$ vs T1) and gradually recovered thereafter, consistent with temporal attenuation of IL-6 signaling. These effects were accompanied by increased secretion of soluble IL-1 receptor type I

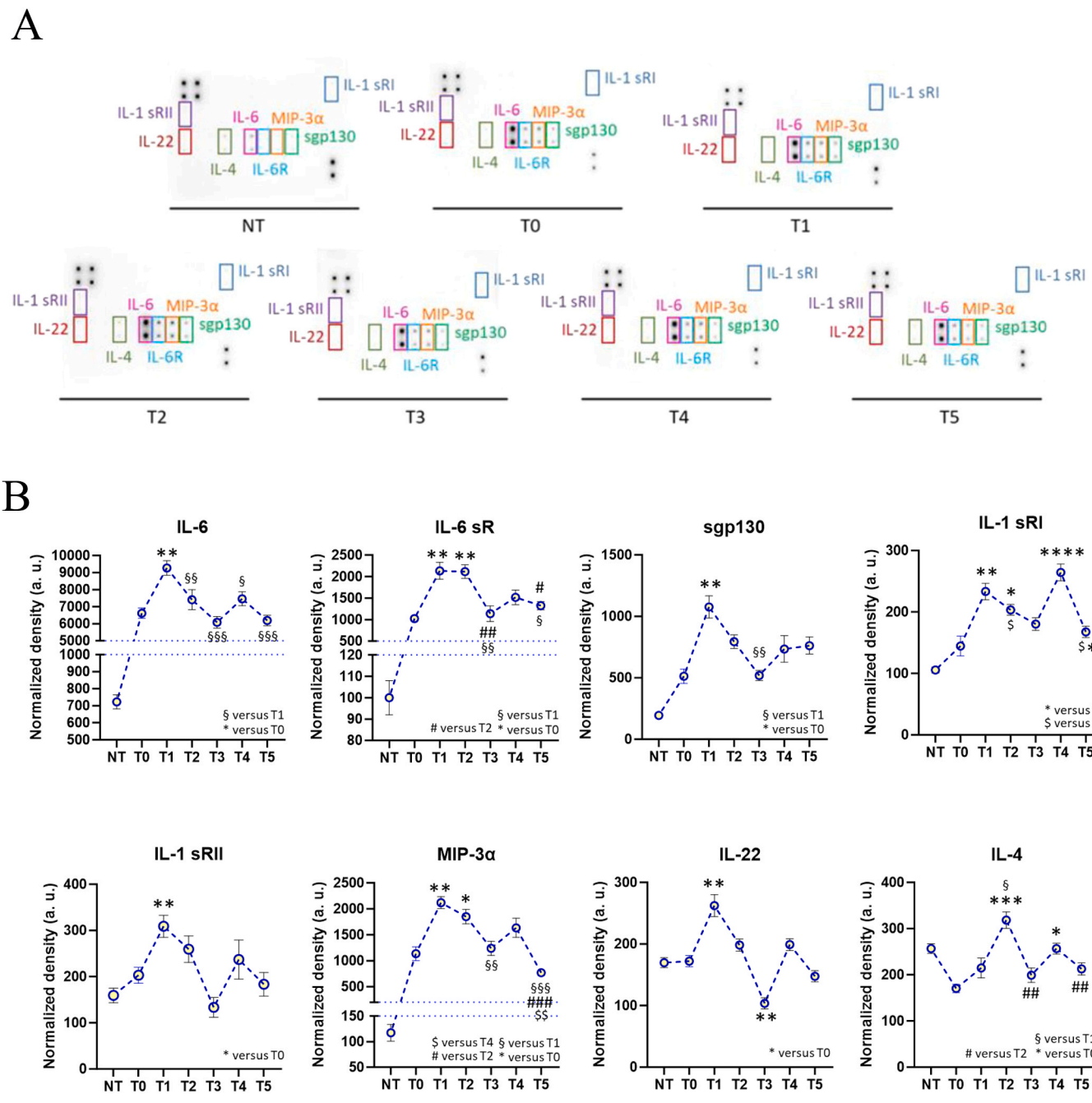

Fig. 3. Semi-quantitative evaluation of cytokine secretion by HUVECs exposed to post-vaccination plasma. Human umbilical vein endothelial cells (HUVECs) were left unstimulated (NT) or stimulated with 10% (v/v) plasma collected longitudinally from healthy vaccinated individuals (T0–T5). Cytokine secretion in supernatants was assessed using a membrane-based antibody array. Increased levels of IL-6, sIL-6R, sgp130, IL-1RI/II, MIP-3α, and IL-22 were observed at early time points (T1–T3), while IL-4 remained low throughout the experimental period. **A-B.** Images of protein arrays and densitometric analysis of spot intensities for selected cytokines reveals distinct temporal patterns of cytokine and soluble receptor secretion. IL-6 and its soluble receptor sIL-6R exhibited a rapid and transient increase, peaking at T1–T2, consistent with an acute-phase systemic response. This was paralleled by a transient decrease in soluble gp130 (sgp130), the natural inhibitor of IL-6 trans-signaling, suggesting temporary disinhibition of the pro-inflammatory IL-6 axis. The chemokine MIP-3α (CCL20), involved in CCR6⁺ leukocyte recruitment, showed early elevation at T1–T2 and returned to baseline by T4, indicating active immune cell trafficking in the immediate post-vaccine phase. IL-22 levels progressively increased and remained elevated at later time points (T3–T4), supporting a role in epithelial barrier maintenance and tissue homeostasis during the resolution phase. In contrast, IL-4 levels remained relatively stable, suggesting absence of Th2-skewed polarization. Together, these findings depict a coordinated, self-limited systemic immune activation, with a distinct transition from early pro-inflammatory signaling to later epithelial-supportive responses.

Table 4
Semiquantitative HUVEC secretome profile across vaccination time points.

Cytokine	NT	T0	T1	T2	T3	T4	T5
IL-6	+	++	+++	+++	++	+	±
IL-6R	±	±	++	++	+	±	±
sgp130	±	±	++	++	+	±	±
IL-1sRI	±	+	++	++	++	+	±
IL-1sRII	±	+	++	++	++	+	±
MIP-3α	±	±	+	++	+	±	±
IL-22	±	±	+	+	±	±	±
IL-4	±	±	±	±	±	±	±

Semi-quantitative evaluation of cytokine secretion by HUVECs cultured under normal condition (not treated, NT) or exposed to pooled plasma from vaccinated individuals longitudinally collected at different time points (T0–T5). Cytokine levels were estimated based on antibody array spot intensity. This visual summary is based on quantitative densitometric data shown in Fig. 3B.
± = barely detectable; + = low intensity; ++ = moderate intensity; +++ = high intensity

Table 5
Primary antibodies used for Western Blot.

Protein Target	Clonality	Host	Dilution	Supplier	Catalog n.
14–3–3 gamma/ YWHAG (EPR9654(B))	Monoclonal	Rabbit	1:1000	Abcam	ab137048
P2Y12 (1C2A9)	Monoclonal	Mouse	1:1000	Abcam	ab233760
ADAMTS13 (EPR6132)	Monoclonal	Rabbit	1:1000	Abcam	ab177940
PAI-1 (D9C4)	Monoclonal	Rabbit	1:1000	Cell Signaling	#11907
β-Actin (D6A8)	Monoclonal	Rabbit	1:2000	Cell Signaling	#8457

Table 6
Primer sequences used for qRT-PCR analysis.

hICAM-1	5' - AGCGGCTGACGTGTGCAGTAAT - 3′
	5' - TCTGAGACCTCTGGCTTCGTCA - 3′
hVCAM-1	5' - GATTCTGTGCCCACAGTAAGGC - 3′
	5' - TGGTCACAGAGCCACCTTCTTG - 3′
hCXCL5	5' – CAGACCACGCAAGGAGTTCATC – 3'
	5' – TTCCTTCCCGTTCTTCAGGGAG – 3'
hMCP-1	5' – AGAATCACCAGCAGCAAGTGTCC – 3'
	5' – TCCTGAACCCACTTCTGCTTGG – 3'
hCD137	5' – TCTTCCTCACGCTCCGTTTCTC – 3'
	5' – TGGAAATCGGCAGCTACAGCCA – 3'
hACTB	5' – CAGCCATGTACGTTGCTATCCAGG – 3'
	5' – AGGTCCAGACGCAGGATGGCATG – 3'

and II (sIL-1RI and sIL-1RII), particularly at T1 ($p < 0.01$), suggesting a rapid activation of regulatory mechanisms involving the IL-1 signaling axis.

Macrophage inflammatory protein-3 alpha (MIP-3α) showed a transient increase at T1 ($p < 0.01$) and T2 ($p < 0.05$), which may indicate the activation of chemoattractant signaling in response to circulating immune mediators.

Importantly, cytokine secretion levels returned close to baseline values at T5, reflecting a self-limited endothelial activation pattern in response to vaccine-induced circulating factors. The observed secretory profile supports a model of transient, non-pathological endothelial stimulation, likely reflecting systemic immune priming rather than vascular injury.

Interestingly, IL-4 and IL-22 displayed biphasic secretion patterns (Fig. 3 B). In particular, IL-22 levels transiently decreased at T2–T3 ($p < 0.01$), followed by partial recovery post-booster, indicating a dynamic alternation between pro- and anti-inflammatory cues. IL-4 levels increased at T2 ($p < 0.001$) following temporal windows consistent with our previous works, in which BNT162b2 vaccination is associated with the activation and/or remodeling of the $CD4^+$ compartment [14].

Overall, the combined behavior of these analytes delineates a finely tuned immune-inflammatory pulse, temporally aligned with systemic platelet remodeling, and ultimately returning to homeostatic values after the second dose, supporting the hypothesis of a self-resolving inflammatory activation tightly coupled to a transient, reversible platelet priming state.

3.4. Early immune activation elicits a transient modulation of endothelial regulatory proteins involved in platelet-associated pathways

To evaluate the balance between pro-activating/pro-thrombotic cues, we performed western blot analysis of the major factors involved in platelet-endothelial cross-talk in HUVECs grown under basal conditions (NT) or exposed to 10% plasma from vaccinated donors (T0-T5): 14–3–3γ (Tyrosine 3-Monooxygenase/Tryptophan 5-Monooxygenase Activation Protein, Gamma Polypeptide) [33], P2Y12 (P2Y purinergic receptor 12) [34], PAI-1 [35,36] and ADAMTS13 (ADAM Metallopeptidase With Thrombospondin Type 1 Motif-13) [37].

In our results (Figs. 4), 14–3–3γ expression displayed an early increase after vaccination (reaching maximal levels at T1–T2, $p < 0.001$ and $p < 0.01$, respectively), followed by a marked reduction from T3 onward ($p < 0.01$), remaining lower throughout the booster phase (T4–T5, $p < 0.01$) (Fig. 4). This adaptor protein family, encoded by the YWHAG gene, binds phospho-serine/threonine motifs on many client proteins and helps coordinate signal transduction, cytoskeletal dynamics and trafficking [38], all processes that are highly relevant to platelet activation/shape change and membrane remodeling. Temporal changes observed in 14–3–3γ protein expression levels may mirror a rapid adaptation of platelet-endothelial signal transduction to vaccination, followed by a restoration of the homeostatic state.

In parallel, P2Y12 expression showed a prominent peak at T1 ($p < 0.0001$), a decline at T3–T4 ($p < 0.05$ vs T1), and a partial rebound at T5 ($p < 0.05$) (Fig. 4). The purinergic receptor P2Y12 amplifies ADP-induced platelet aggregation and modulates platelet-endothelial interactions and inflammatory responses. Dynamic regulation of P2Y12 levels may indicate an early transient activation of platelet–endothelial inflammatory signalling, with first vaccination exposure triggering a higher platelet-vascular response and subsequent booster administration leading to a more limited response.

PAI-1, a key regulator of the equilibrium between coagulation and fibrinolysis, exhibited a delayed but robust rise, peaking at T2 ($p < 0.01$), followed by a pronounced decrease at later time points (T3–T5, $p < 0.0001$), providing insight into a transient modulation of fibrinolytic and inflammatory pathways that self-resolves over time. However, the ADAMTS13 immunoreactive signal increased progressively from T2, reaching its highest levels during the booster/early post-booster interval (T4–T5, $p < 0.05$). Given that this metalloprotease is responsible for cleaving ultra-large von Willebrand factor (vWF) released from endothelium and thereby inhibiting platelet adhesion, its delayed induction may reflect a compensatory antithrombotic response at the endothelial–platelet interface (Fig. 4).

Collectively, these data indicate a time-resolved remodeling of platelet-associated signalling pathways, consisting of early priming-linked changes in 14–3–3γ and P2Y12 and a distinct mid-course peak in PAI-1, contrasted by a later increase in ADAMTS13 levels (Fig. 4).

This result supports transcriptional findings and suggests that early immune activation elicits a transient elevation of key endothelial regulatory proteins involved in intracellular signaling. In particular, the increased expression of 14–3–3γ in HUVECs following exposure to post-vaccination plasma highlights the involvement of cytoplasmic signaling hubs in endothelial adaptation to immune stimuli. The 14–3–3 family of phospho-serine/threonine-binding proteins is known to regulate multiple intracellular pathways, including PI3K/Akt and MAPK/ERK [39,40], which are activated downstream of both IL-6 trans-signaling and

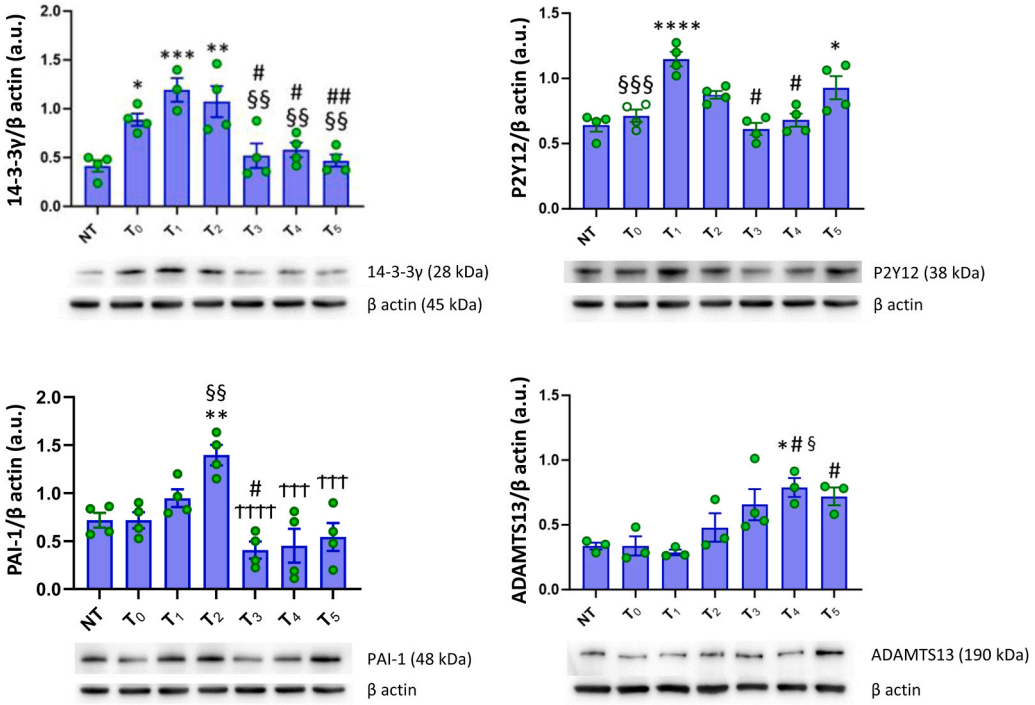

Fig. 4. Immunoblot analysis of thrombo-inflammatory protein expression in HUVECs exposed to post-vaccination plasma. Representative Western blot of the complementary nodes of platelet thrombo-inflammatory regulation (14–3-3γ, P2Y12, PAI-1, ADAMTS13) during the immunization timeline, showing protein expression in HUVECs unstimulated (NT) or stimulated for 6 h with 10% pooled plasma from vaccinated individuals (T0-T5). For each time point, plasma samples were combined into two independent pools, each derived from three different donors longitudinally followed throughout the study. Each condition was tested in duplicate, and the stimulation experiment was independently repeated twice. A transient early increase in 14–3-3γ and P2Y12 protein levels was observed from T1, with both markers returning to baseline by T3. However, PAI-1 protein levels increased at T2 and returned to baseline at T3. Interestingly, ADAMTS13 showed a delayed increase, reaching its highest levels during the booster phase (T4-T5). These findings suggest temporally regulated endothelial sensitization to purinergic signaling in response to systemic vaccine-induced cues. β-actin served as a loading control. Data are presented as mean ± SEM; Statistical analysis was performed using one-way ANOVA followed by Tukey's multiple-comparisons test for 14–3-3γ (* versus NT; § versus T1; # versus T2); P2Y12 (* versus NT; § versus T1: # versus T1); PAI-1 (* versus NT; § versus T0; # versus T1; † versus T2); ADAMTS13 (* versus NT; § versus T0; # versus T1).

CD40/CD40L interactions [41,42]. Its transient upregulation may thus reflect a controlled endothelial priming state, capable of integrating immune-derived cues into adaptive and pro-survival responses while preserving endothelial homeostasis and avoiding overt dysfunction.

3.5. Early immune activation elicits a transient modulation of endothelial inflammatory and adhesion-related genes

To further characterize the endothelial response induced by vaccine administration, we stimulated HUVECs with 10% plasma from vaccinated subjects (T0–T5) and assessed the expression of genes involved in endothelial activation, leukocyte recruitment, and inflammatory signaling by RT-qPCR (Fig. 5).

ICAM-1, a key adhesion molecule critically involved in leukocyte transmigration and endothelial activation, showed an early and transient upregulation after the first vaccine dose, reaching a maximum at T1 ($p < 0.05$ vs T0), followed by a rapid return to baseline levels at T2 (< 0.05 vs T1). The endothelial activation marker VCAM-1 progressively increased throughout the immunization period, peaking at T4 ($p < 0.05$ vs T0) and subsequently declined to baseline at T5 ($p < 0.05$ vs T4), consistent with a transient enhancement of endothelial responsiveness following vaccination without occurrence of sustained activation.

Interestingly, expression of CD137, a costimulatory receptor involved in endothelial-immune cell crosstalk, increased during the vaccination time course, with significantly higher levels at T4 compared with baseline and early post-vaccination time points ($p < 0.01$ vs T0 and $p < 0.05$ vs T1). This delayed induction may reflect the establishment of adaptive immune signalling pathways associated with booster immunization.

CXCL5, a neutrophil chemoattractant implicated in inflammatory cell recruitment, showed a delayed increase, with the maximum at T3 ($p < 0.01$ vs T0) and returned to baseline values at the last time point ($p < 0.05$ vs T3), supporting a transient induction of chemotactic signals following the acute post-vaccination phase.

In contrast, MCP-1, a chemokine involved in monocyte recruitment and chronic vascular inflammation, progressively decreased throughout the vaccination time course, with significantly lower levels at T4–T5 compared with baseline ($p < 0.01$ and $p < 0.05$ vs T0, respectively). Given the role of MCP-1 in monocyte recruitment and chronic vascular inflammation, its downregulation reinforce a transient activation of selected inflammatory pathways in the absence of sustained endothelial dysfunction.

Overall, these data support the concept that plasma from vaccinated individuals induces a dynamic and tightly regulated endothelial response characterized by transient modulation of adhesion and inflammatory mediators. Importantly, the transcriptional changes parallel the temporal remodeling of platelet ultrastructure and cytokine secretion explained above, reinforcing our hypothesis that BNT162b2 vaccination promotes a physiological and reversible endothelial activation state associated with immune priming rather than sustained inflammation.

4. Discussion

In this longitudinal study, we provide evidence of a transient endothelial activation program occurring in parallel with platelet structural and functional remodelling, using a human model of BNT162b2 mRNA immunization. The main conceptual advance is that platelet responses

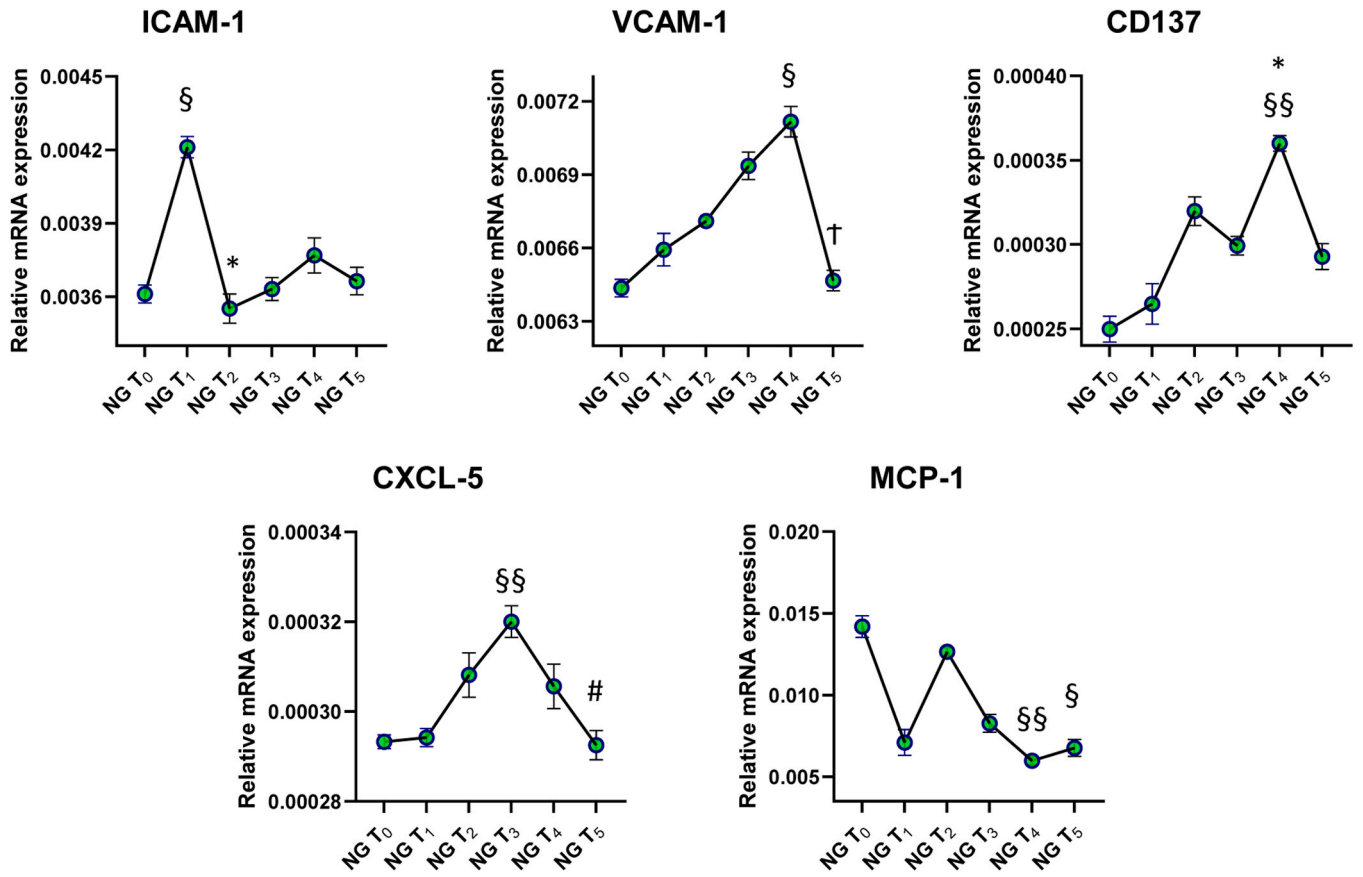

Fig. 5. RT-qPCR analysis of endothelial activation-related gene expression in HUVECs stimulated with post-vaccination plasma. HUVECs were left unstimulated (NT) or stimulated for 6 h with 10% pooled plasma collected from healthy volunteers before (T0) and at the indicated time points after vaccination (T1-T5). Two independent plasma pools were generated for each time point, each derived from three distinct longitudinally followed donors. Each condition was tested in duplicate, and the entire stimulation experiment was performed in two independent runs. Gene expression levels of ICAM-1, V-CAM1, CD137, CXCL5 and MCP-1 were quantified by RT-qPCR. Trascriptional levels of ICAM-1 showed an early upregulation after the first vaccination dose, while CXCL5 increased during the intermediate time points and VCAM-1 and CD137 peaked at T4, before returning to baseline levels at T5. Conversely, MCP-1 was downregulated concomitant with the two vaccination doses. These data are consistent with a dynamic and tightly regulated endothelial response induced by post-vaccination plasma and characterized by transient modulation of adhesion and inflammatory mediators rather than sustained endothelial dysfunction. Results were normalized to β-actin using the ΔCt method and reported as relative expression ($2^{-\Delta Ct}$). Data are presented as mean ± SEM (n = 4 independent biological replicates, corresponding to two independent experimental runs, each including two plasma pools). Statistical analysis was performed using one-way ANOVA followed by Tukey's multiple comparisons test for ICAM-1 (§ vs T0; * vs T1), V-CAM1 (§ vs T0; † vs T4), CD137 (§ vs T0; * vs T1), CXCL5 (§ vs T0; # vs T3), and MCP-1 (§ vs T0).

during immunization are not fully captured by conventional activation markers alone, but instead may follow a sequential remodeling trajectory that is detectable at the subcellular level. By integrating TEM-derived endpoints, such as OCS area and αG number (Fig. 1), with soluble mediators and endothelial markers, we delineate a candidate morpho-functional platelet signature consistent with physiological priming rather than maladaptive thrombo-inflammation [43,44].

A first key finding is the presence of transient OCS expansion and αG depletion across the prime–boost immunization protocol. OCS enlargement is mechanistically plausible as an early structural correlate of increased membrane reserve and trafficking capacity, supporting rapid surface remodeling and regulated secretion [17–19]. The OCS is an elaborate tunneling network of membrane invaginations and surface-connected channels that is unique to platelets. Besides its functions as a pathway for the transport of substances into platelets and as a conduit for the release of αG products upon platelet activation [18], the OCS acts as a membrane reservoir that can rapidly evaginate after platelet activation, contributing to changes in platelet shape and to an increased surface area-to-volume ratio [19].

Conversely, a reduction in αG number is consistent with either partial release, redistribution, or altered granule packing during intermediate activation states. αGs are the most abundant platelet secretory granules; *King et al.* estimated a content of approximately 80 αGs per platelet [16], with sizes ranging from 200 to 500 nm. They originate from biosynthetic pathways of the trans-Golgi network [45] and account for nearly 10% of platelet volume, with a total membrane surface area approximately equal to that of the OCS. Importantly, we observed these ultrastructural dynamics in the context of stable clinical physiology: platelet counts fluctuated after each vaccine dose but remained within the normal range (Fig. 2 C), and no overt sustained secretory pattern emerged for P-selectin (Fig. 2 D). Notably, αGs content, platelet counts, and P-selectin secretion are focal points for the definition of platelet activation state.

Despite no functional platelet activity assays were performed, together these data support a model in which platelets may undergo reversible adaptation, structurally preparing for activation without necessarily transitioning into a persistent degranulated phenotype.

P-selectin is particularly informative because it is traditionally associated with αG secretion. Although αG depletion and OCS expansion suggest engagement of the secretory apparatus, P-selectin levels did not show a sustained increase and even tended to decrease after the second dose, returning toward baseline thereafter. This dissociation supports the concept of a primed/intermediate activation state, in which platelets are functionally sensitized and structurally remodelled but not

persistently αG secreting. This phenotype is recognized in settings of low-grade inflammatory stimulation, where platelets can modulate vascular and immune crosstalk through contact-dependent mechanisms (e.g., receptor engagement, microvesicle release) without engaging the full αG secretion profile typically associated with thrombo-inflammation [46,47].

The expansion of OCS is critical for platelet spreading, as demonstrated by studies in bovine platelets, which lack the extensive OCS characteristic of human platelets but can rapidly extrude channels upon stimulation [48]. Our results corroborate the concept that platelets can increase their surface area by 2- to 4-fold upon stimulation [17]. Indeed, our findings reveal a temporal association between increased OCS area at particular time-points, specifically at T1-T3, and changes in platelet parameters, suggesting an increase in the membrane exchange surface (with minor effects on the platelet volume, as shown by MPV). This interpretation is further corroborated by the associations observed with platelet-specific parameters, including P-LCR [49], PDW and MPV (Table 3). In particular, P-LCR is susceptible to alterations in platelet size [28] (Table 3), which may explain its association with thrombogenic potential. Indeed, P-LCR probably identifies those platelets that are metabolically and enzymatically more active, relatively younger and contain more intracellular granules than smaller platelets. As a result, OCS expansion could be interpreted as a transient stage of platelet activation, a concept that is further supported by the reduction in OCS area observed at T4 and T5 (Fig. 1 B-C).

This transient platelet activation is lost after the second vaccination dose, as highlighted by our results on αG release, assessed by measurement of serum P-selectin levels, which were reduced at T4. We and others have observed a positive association between αG number and platelets count [50], consistent with the results in Table 2.

In addition, the increase of systemic inflammation markers, such as NLR and PLR, although surrogate markers, demonstrated the presence of a transient inflammation throughout the whole immunization process.

These findings are consistent with our previous study demonstrating that SARS-CoV-2 mRNA vaccination induced a marked and persistent expansion of IFNγ-producing NK and T cells in healthy individuals [14], accompanied by alterations in hematological parameters [53] and in the distribution of lymphocytic subpopulations, with a particular phenotypic profile characterized by a prevalence of natural killer (NKs) cells and CD19 + B cells.

Systemic mediator profiling further supports a transient inflammatory role for circulating IL-6. The temporal correlation between lymphocyte activation [14] and levels of circulating inflammatory mediators (e.g., IL-6, IL-1R, IL-22) observed in our results (Fig. 3) supports the hypothesis that transient endothelial and platelet activation may be partially driven by vaccine-induced immune remodeling involving innate lymphoid cells. The modulation of sgp130 suggests the activation of feedback mechanisms that buffer IL-6 signaling, consistent with a controlled, non-pathological inflammatory response. In parallel, the transient elevation of MIP-3α may reflect early chemoattractant signaling from activated endothelium, potentially supporting leukocyte recruitment in the immediate post-vaccine phase.

RT-qPCR analysis provides functional evidence that post-vaccination plasma induced a coordinated but self-limited modulation of endothelial cell transcriptional programs in HUVECs (Fig. 5). The rapid induction of ICAM-1, followed by its rapid normalization, is consistent with a transient increase in endothelial adhesiveness and leukocyte attraction potential during the early post-vaccination immune response. Conversely, the gradual increase in VCAM-1, peaking at T4, suggests that endothelial responsiveness dynamically evolves throughout the immunization period, in parallel with the maturation of the adaptive immune response. This interpretation is further supported by the delayed upregulation of CD137, which may reflect the emergence of adaptive immune signaling following booster immunization. The gene expression profile also revealed a selective regulation of chemokine pathways: CXCL5 is transiently upregulated during the intermediate post-vaccination phase, consistent with a temporary enhancement of chemotactic signaling, whereas MCP-1 is progressively reduced during the immunization phase, evidencing the absence of a persistent pro-inflammatory endothelial activation state.

Notably, these endothelial transcriptional changes closely paralleled the transient alterations found in platelet ultrastructure and circulating inflammatory mediators. The early induction of adhesion molecules coincides with the phase of OCS expansion and α-granule depletion, whereas the subsequent normalization of endothelial gene expression accompanies the recovery of platelet ultrastructural parameters. Together, these observations support a model in which vaccine-induced immune activation transiently coordinates tightly regulated and rapidly resolved endothelial and platelet responses, limiting prolonged inflammation and preserving endothelial homeostasis (Supplementary Fig. S2).

Finally, the modulation of platelet-associated proteins linked to thrombo-inflammatory balance (including P2Y12, PAI-1, and ADAMTS13) suggests that the host response integrates not only pro-activating cues but also counter-regulatory adjustments that may favour rapid resolution of the inflammatory response (Fig. 4). mRNA vaccination triggers a transient activation of the vascular compartment, characterized by early signs of platelet priming (OCS expansion and αG changes), regulated endothelial activation (14–3–3γ and P2Y12 signaling), and a compensatory antithrombotic response (ADAMTS13 signaling). Platelets initially displayed increased activation readiness; next, they reach a peak in pro-thrombo-inflammatory and fibrinolytic signals. Finally, a compensatory response appears to emerge, marked by the upregulation of negative regulators such as ADAMTS13, which is known to proteolytically cleave ultra-large vWF multimers, thereby limiting vWF-dependent platelet tethering and adhesion [51,52]. Although these experiments were performed in an in vitro model that cannot fully recapitulate the complexity of the in vivo vascular environment, they provide mechanistic support for the concept that immune responses generated during immunization are sufficient to induce a reversible endothelial activation program rather than sustained endothelial injury.

Taken together, these data argue that OCS and αG dynamics capture a highly sensitive window into platelet participation in a transient and reversible, vaccine-driven systemic inflammatory state, offering a conceptual framework to understand why, in most healthy individuals, platelet perturbation is self-limited, while also highlighting ultrastructural endpoints that could be investigated in populations at higher thrombo-inflammatory risk.

In addition, reduced platelet production is usually caused by a bone marrow defect, which would also affect the production of red blood cells and leukocytes. In our previous observations [14], lymphocytes count, but not erythrocytes count, showed the same trend as the platelet count (Supplementary Fig. S3). At T1, the number of granules is proportional to the number of platelets, i.e. platelets counts decrease in parallel with αG number. Thus, platelet activation may prove as a potential biomarker for predicting, diagnosing, and managing side effects of vaccines, although little is known about the mechanisms that initiate and sustain platelet activation in side effects of vaccination, or how platelets may be involved in the pathogenesis of hemostatic abnormalities.

Our longitudinal analysis identifies a candidate platelet phenotype occurring in response to BNT162b2 immunization, interpretable as transient, reversible ultrastructural priming rather than full-blown degranulation. The most informative signature emerges from TEM-based analysis: during the inter-dose interval, platelets exhibit a marked remodeling of the OCS, accompanied by a reduction in αG number, with both parameters returning toward baseline after completion of the two-dose schedule. Notably, this remodeling unfolds in parallel with a systemic inflammatory pulse, as suggested by IL-6 kinetics and by the temporal behavior of NLR/PLR, thereby supporting a model in which vaccine-induced inflammation transiently re-sets the platelet "activation threshold." Importantly, the absence of

ultrastructural evidence of viral particles within platelets reinforces the notion that the observed phenotype is driven by immune activation rather than direct viral interaction. A seemingly paradoxical element—the lack of a concordant increase in soluble P-selectin and the reduction in circulating CD40L—actually strengthens the mechanistic interpretation: platelets appear to adopt an intermediate activation state characterized by membrane and canalicular rearrangement and granule compartment reorganization, without a sustained systemic secretory footprint typical of canonical αG release.

In conclusion, platelet ultrastructural organization may offer a mechanistically informative complement to soluble and surface biomarkers. Two compartments appear particularly relevant in this structural plasticity: αG, which store a broad repertoire of hemostatic and immunomodulatory mediators, and OCS, a surface-connected membrane network that supports trafficking, secretion routes, and rapid changes in membrane availability. Because the platelet priming state may involve membrane remodeling and organelle redistribution without sustained degranulation or full activation, it is possible that ultrastructural morphometrics may capture aspects of platelet adaptation that are not fully reflected by platelet count or soluble P-selectin readouts.

In this setting, TEM enables direct quantification of αG content and OCS remodeling, providing a time-resolved structural framework to interpret platelet–vascular responses to vaccine-induced immune activation.

Importantly, our study was designed as a longitudinal within-subject investigation, in which blood samples were collected from each participant prior to the administration of the mRNA-based BNT162b2 vaccine and repeatedly after vaccination. Therefore, our study establishes a clear temporal sequence between vaccine administration and observed outcomes. It should be noted that current study is not without limitations, because the follow-up was limited to only 5 weeks after the first vaccine administration and direct platelet functional assays were absent.

While the observed temporal associations support the concept of reversible platelet remodeling during vaccination, further studies are required to demonstrate the mechanistic pathways underlying this model and to determine whether OCS and αG morphometric parameters provide independent discriminatory or predictive value in clinically relevant thrombo-inflammatory conditions. Future investigations integrating functional platelet assays, larger longitudinal cohorts, and disease-specific models will be necessary to establish whether these ultrastructural features represent generalizable biomarkers of platelet adaptation or, conversely, markers of pathological platelet activation.

CRediT authorship contribution statement

Francesca Rispoli: Writing – review & editing, Formal analysis. **D'Anzeo marco:** Writing – review & editing, Data curation. **Macas Granizo Maria:** Writing – review & editing, Formal analysis. **Lucia La Sala:** Writing – original draft, Supervision, Methodology, Data curation, Conceptualization. **Angelo Naselli:** Writing – review & editing, Data curation. **Emilio Trabucchi:** Conceptualization. **Valentina Carlini:** Writing – original draft, Methodology, Investigation, Formal analysis, Data curation. **Cesare Berra:** Writing – review & editing, Data curation. **Elena Tagliabue:** Writing – review & editing, Data curation. **Norma Lattuada:** Writing – review & editing, Formal analysis, Data curation. **Alberto Settembrini:** Writing – review & editing, Supervision, Data curation. **Nadia Santo:** Formal analysis, Data curation. **Raffaele Allevi:** Writing – review & editing, Formal analysis, Data curation. **Elena Dozio:** Writing – review & editing, Validation, Data curation. **Elena Vianello:** Writing – review & editing, Validation, Formal analysis, Data curation. **Stefania Saccucci:** Writing – review & editing, Formal analysis, Data curation. **Massimiliano Corsi Romanelli:** Writing – review & editing, Supervision, Methodology, Data curation. **Ermanno Longhi:** Writing – review & editing, Formal analysis, Data curation. **Martino Bolognesi:** Writing – review & editing, Supervision, Methodology, Formal analysis, Data curation, Conceptualization. **Barbara Bianchi:** Writing – review & editing, Formal analysis, Data curation. **Pontiroli Antonio:** Writing – review & editing, Formal analysis, Data curation.

Author Contributions

VC, ET, NS, NL, SS, RA, FR, BB, EL, MBMG, MD'A, CB, AN, AS, EV, ED, ETa, MCR, AEP, MB, LLS. Conceptualization: ET, LLS. Writing—original draft preparation: VC, LLS. Writing—review and editing: ET, NS, NL, SS, FR, BB, EL, MBMG, MD'A, CB, AN, AS, EV, ED, ETa, MCR, AEP, MB. Formal analysis and figure preparation: VC, LLS, NS, NL, SS, RA. All authors have read and agreed to the published version of the manuscript.

Institutional Review Board Statement

The study was conducted according to the guidelines of the Declaration of Helsinki and approved by the Independent Ethics Committee of IRCCS MultiMedica, Milan (application number 470.2021, CE-40.2021).

Informed Consent Statement

Informed consent was obtained from all subjects involved in the study.

Declaration of Competing Interest

All authors declare that they have no known financial interests or personal relationships that could have appeared to influence the work reported in this manuscript. The authors confirm that there are no conflicts of interest associated with this publication.

Acknowledgments

This work has been supported by "Ricerca Corrente" of the Italian Ministry of Health to IRCCS MultiMedica, Milan, Italy. The authors would like to thank Fondazione Romeo and Enrica Invernizzi, Milan, Italy, for the support. We are also grateful for the support received from all the personnel involved in this study, all from the Department of Medicina del Lavoro at IRCCS MultiMedica, and the Office for Preventive Medicine. We thank Ms Elisabetta Gualtieri, Ms Monica Pivatello, Ms Francesca Lehman, Mr Luca Carissimi for their technical assistance in sample processing.

Appendix A. Supporting information

Supplementary data associated with this article can be found in the online version at doi:10.1016/j.biopha.2026.119961.

Data availability

Data will be made available on request.

References

[1] K. Kaushansky, The molecular mechanisms that control thrombopoiesis, J. Clin. Invest. 115 (12) (2005) 3339–3347.
[2] P. von Hundelshausen, C. Weber, Platelets as immune cells: bridging inflammation and cardiovascular disease, Circ. Res. 100 (1) (2007) 27–40.
[3] P. Cunin, P.A. Nigrovic, Megakaryocytes as immune cells, J. Leukoc. Biol. 105 (6) (2019) 1111–1121.
[4] A. Finkielsztein, et al., Human megakaryocyte progenitors derived from hematopoietic stem cells of normal individuals are MHC class II-expressing professional APC that enhance Th17 and Th1/Th17 responses, Immunol. Lett. 163 (1) (2015) 84–95.
[5] A. Zufferey, et al., Mature murine megakaryocytes present antigen-MHC class I molecules to T cells and transfer them to platelets, Blood Adv. 1 (20) (2017) 1773–1785.

[6] S.A. Crist, et al., Early growth response-1 (EGR-1) and nuclear factor of activated T cells (NFAT) cooperate to mediate CD40L expression in megakaryocytes and platelets, J. Biol. Chem. 288 (47) (2013) 33985–33996.
[7] R.A. Campbell, et al., Human megakaryocytes possess intrinsic antiviral immunity through regulated induction of IFITM3, Blood 133 (19) (2019) 2013–2026.
[8] M.B. Vogt, et al., Dengue viruses infect human megakaryocytes, with probable clinical consequences, PLoS. Negl. Trop. Dis. 13 (11) (2019) e0007837.
[9] S. Shen, et al., SARS-CoV-2 interacts with platelets and megakaryocytes via ACE2-independent mechanism, J. Hematol. Oncol. 14 (1) (2021) 72.
[10] E. Davoudi-Monfared, et al., A Randomized Clinical Trial of the Efficacy and Safety of Interferon beta-1a in Treatment of Severe COVID-19, Antimicrob. Agents Chemother. 64 (9) (2020).
[11] M.J. Mulligan, et al., Phase I/II study of COVID-19 RNA vaccine BNT162b1 in adults, Nature 586 (7830) (2020) 589–593.
[12] U. Sahin, et al., COVID-19 vaccine BNT162b1 elicits human antibody and T(H)1 T cell responses, Nature 586 (7830) (2020) 594–599.
[13] F.P. Polack, et al., Safety and Efficacy of the BNT162b2 mRNA Covid-19 Vaccine, N. Engl. J. Med. 383 (27) (2020) 2603–2615.
[14] L. La Sala, et al., SARS-CoV-2 Immunization Orchestrates the Amplification of IFNgamma-Producing T Cell and NK Cell Persistence, Front. Immunol. 13 (2022) 798813.
[15] E. Galeota, et al., Tracking the immune response profiles elicited by the BNT162b2 vaccine in COVID-19 unexperienced and experienced individuals, Clin. Immunol. 261 (2024) 110164.
[16] S.M. King, G.L. Reed, Development of platelet secretory granules, Semin. Cell. Dev. Biol. 13 (4) (2002) 293–302.
[17] P. Blair, R. Flaumenhaft, Platelet alpha-granules: basic biology and clinical correlates, Blood Rev. 23 (4) (2009) 177–189.
[18] G. Escolar, J.G. White, The platelet open canalicular system: a final common pathway, Blood Cells 17 (3) (1991) 467–485, discussion 486-95.
[19] J.G. White, C.C. Clawson, The surface-connected canalicular system of blood platelets–a fenestrated membrane system, Am. J. Pathol. 101 (2) (1980) 353–364.
[20] J.G. White, Electron microscopy methods for studying platelet structure and function, Methods Mol. Biol. 272 (2004) 47–63.
[21] F. Tondi, et al., Hermansky-Pudlak Syndrome: From Molecular Pathogenesis to Targeted Therapies, IUBMB Life 77 (5) (2025) e70025.
[22] L. Sereni, et al., Autonomous role of Wiskott-Aldrich syndrome platelet deficiency in inducing autoimmunity and inflammation, J. Allergy Clin. Immunol. 142 (4) (2018) 1272–1284.
[23] S. Greene, et al., Chediak-Higashi Syndrome: Hair-to-toe spectrum, Semin. Pediatr. Neurol. 52 (2024) 101168.
[24] M. Gunay-Aygun, et al., Gray platelet syndrome: natural history of a large patient cohort and locus assignment to chromosome 3p, Blood 116 (23) (2010) 4990–5001.
[25] C. Garcia, et al., SARS-CoV-2 Omicron variant infection affects blood platelets, a comparative analysis with Delta variant, Front. Immunol. 14 (2023) 1231576.
[26] J.F. Theoret, et al., P-selectin ligation induces platelet activation and enhances microaggregate and thrombus formation, Thromb. Res. 128 (3) (2011) 243–250.
[27] K.L. Kaplan, et al., Platelet alpha-granule proteins: studies on release and subcellular localization, Blood 53 (4) (1979) 604–618.
[28] Y. Gao, et al., The impact of various platelet indices as prognostic markers of septic shock, PLoS. One 9 (8) (2014) e103761.
[29] S. Kaur, et al., Upregulation of cytokine signalling in platelets increases risk of thrombophilia in severe COVID-19 patients, Blood Cells Mol. Dis. 94 (2022) 102653.
[30] S.A. Burstein, Cytokines, platelet production and hemostasis, Platelets 8 (2-3) (1997) 93–104.
[31] F. Cognasse, et al., Platelets as Key Factors in Inflammation: Focus on CD40L/CD40, Front. Immunol. 13 (2022) 825892.
[32] C. Aloui, et al., The signaling role of CD40 ligand in platelet biology and in platelet component transfusion, Int. J. Mol. Sci. 15 (12) (2014) 22342–22364.
[33] L. Marsal-Garcia, et al., 14-3-3sigma up-regulation in the temporal cortex associates with tau pathology and reactive astroglia in Lewy body disorders, Brain Pathol. (2025) e70059.
[34] I.A. Muravlev, O.A. Antonova, A.V. Mazurov, Effects of cyclooxygenase and P2Y12 ADP receptor inhibitors on platelet phosphatidylserine exposure in vitro and in vivo, Blood Coagul. Fibrinolysis 37 (2) (2026) 56–59.
[35] X. Xu, et al., PAI-1 promotes thromboangiitis obliterans progression through NF-kappaB-NLRP3 pathway activation via HIF-1alpha-dependent signaling, Microvasc. Res. 163 (2026) 104885.
[36] D.E. Vaughan, PAI-1 and atherothrombosis, J. Thromb. Haemost. 3 (8) (2005) 1879–1883.
[37] S.J. Humphreys, N.J. Mutch, C.S. Whyte, Endothelial cell source dictates the expression and release of fibrinolytic markers in a proinflammatory environment, Res. Pract. Thromb. Haemost. 9 (5) (2025) 102929.
[38] A. Boudreau, et al., 14-3-3sigma stabilizes a complex of soluble actin and intermediate filament to enable breast tumor invasion, Proc. Natl. Acad. Sci. USA 110 (41) (2013) E3937–E3944.
[39] T. Obsil, V. Obsilova, Structural basis of 14-3-3 protein functions, Semin. Cell. Dev. Biol. 22 (7) (2011) 663–672.
[40] V.M. Radhakrishnan, J.D. Martinez, 14-3–3 gamma induces oncogenic transformation by stimulating MAP kinase and PI3K signaling, PLoS. One 5 (7) (2010) e11433.
[41] M.M. Zegeye, et al., Activation of the JAK/STAT3 and PI3K/AKT pathways are crucial for IL-6 trans-signaling-mediated pro-inflammatory response in human vascular endothelial cells, Cell. Commun. Signal. 16 (1) (2018) 55.
[42] T. Tang, et al., Molecular basis and therapeutic implications of CD40/CD40L immune checkpoint, Pharmacol. Ther. 219 (2021) 107709.
[43] E. Lutgens, et al., Requirement for CD154 in the progression of atherosclerosis, Nat. Med. 5 (11) (1999) 1313–1316.
[44] A. Afek, et al., Clopidogrel attenuates atheroma formation and induces a stable plaque phenotype in apolipoprotein E knockout mice, Microvasc. Res. 77 (3) (2009) 364–369.
[45] E.M. Cramer, et al., Uncoordinated expression of alpha-granule proteins in human megakaryocytes, Prog. Clin. Biol. Res. 356 (1990) 131–142.
[46] K.Y. Stokes, D.N. Granger, Platelets: a critical link between inflammation and microvascular dysfunction, J. Physiol. 590 (5) (2012) 1023–1034.
[47] A. Veninga, et al., Effects of Platelet Agonists and Priming on the Formation of Platelet Populations, Thromb. Haemost. 122 (5) (2022) 726–738.
[48] J.G. White, The secretory pathway of bovine platelets, Blood 69 (3) (1987) 878–885.
[49] J.D. Bessman, L.J. Williams, P.R. Gilmer, Jr., *Mean platelet volume. The inverse relation of platelet size and count in normal subjects, and an artifact of other particles.* Am. J. Clin. Pathol. 76 (3) (1981) 289–293.
[50] T.M. Quinton, et al., Different G protein-coupled signaling pathways are involved in alpha granule release from human platelets, J. Thromb. Haemost. 2 (6) (2004) 978–984.
[51] I. Mancini, et al., FRETS-VWF73 rather than CBA assay reflects ADAMTS13 proteolytic activity in acquired thrombotic thrombocytopenic purpura patients, Thromb. Haemost. 112 (2) (2014) 297–303.
[52] J.F. Dong, et al., ADAMTS-13 rapidly cleaves newly secreted ultralarge von Willebrand factor multimers on the endothelial surface under flowing conditions, Blood 100 (12) (2002) 4033–4039.
[53] L. LA SALA, et al., Evaluation of hematological abnormalities in subjects vaccinated with BNT162b2 in a longitudinal cohort of the CORE study, La Riv. Ital. della Med. di Lab. (2022).

Further reading

[1] K.F. Larson, et al., Myocarditis After BNT162b2 and mRNA-1273 Vaccination, Circulation 144 (6) (2021) 506–508.
[2] C.M. Rosner, et al., Myocarditis Temporally Associated With COVID-19 Vaccination, Circulation 144 (6) (2021) 502–505.
[3] S. Abu Mouch, et al., Myocarditis following COVID-19 mRNA vaccination, Vaccine 39 (29) (2021) 3790–3793.
[4] N. Mercade-Besora, et al., The role of COVID-19 vaccines in preventing post-COVID-19 thromboembolic and cardiovascular complications, Heart 110 (9) (2024) 635–643.
[5] N. Pardi, et al., Expression kinetics of nucleoside-modified mRNA delivered in lipid nanoparticles to mice by various routes, J. Control. Release 217 (2015) 345–351.
[6] U. Sahin, K. Kariko, O. Tureci, mRNA-based therapeutics–developing a new class of drugs, Nat. Rev. Drug. Discov. 13 (10) (2014) 759–780.
[7] A.B. Vogel, et al., BNT162b vaccines protect rhesus macaques from SARS-CoV-2, Nature 592 (7853) (2021) 283–289.
[8] L. La Sala, et al., Metabolic disorders affecting the liver and heart: Therapeutic efficacy of miRNA-based therapies? Pharmacol. Res. 201 (2024) 107083.
[9] I.S. Fernandez, et al., Unusual base pairing during the decoding of a stop codon by the ribosome, Nature 500 (7460) (2013) 107–110.
[10] S. Amit, et al., Early rate reductions of SARS-CoV-2 infection and COVID-19 in BNT162b2 vaccine recipients, Lancet 397 (10277) (2021) 875–877.
[11] H. Kouhpayeh, H. Ansari, Adverse events following COVID-19 vaccination: A systematic review and meta-analysis, Int. Immunopharmacol. 109 (2022) 108906.
[12] S. Mansanguan, et al., Cardiovascular Manifestation of the BNT162b2 mRNA COVID-19 Vaccine in Adolescents, Trop. Med. Infect. Dis. 7 (8) (2022).
[13] W. Woo, et al., Clinical characteristics and prognostic factors of myocarditis associated with the mRNA COVID-19 vaccine, J. Med. Virol. 94 (4) (2022) 1566–1580.
[14] G. Witberg, et al., Myocarditis after Covid-19 Vaccination in a Large Health Care Organization, N. Engl. J. Med. 385 (23) (2021) 2132–2139.
[15] B. Bozkurt, I. Kamat, P.J. Hotez, Myocarditis With COVID-19 mRNA Vaccines, Circulation 144 (6) (2021) 471–484.
[16] K. Kariko, et al., Suppression of RNA recognition by Toll-like receptors: the impact of nucleoside modification and the evolutionary origin of RNA, Immunity 23 (2) (2005) 165–175.
[17] S.R. Ostrowski, et al., Inflammation and Platelet Activation After COVID-19 Vaccines - Possible Mechanisms Behind Vaccine-Induced Immune Thrombocytopenia and Thrombosis, Front. Immunol. 12 (2021) 779453.
[18] N. Gerdes, et al., Platelet CD40 Exacerbates Atherosclerosis by Transcellular Activation of Endothelial Cells and Leukocytes, Arterioscler. Thromb. Vasc. Biol. 36 (3) (2016) 482–490.